Available online at www.sciencedirect.com
SCIENCE DIRECT
Journal of Sound and Vibration 293 (2006) 933–943
JOURNAL OF SOUND AND VIBRATION
www.elsevier.com/locate/jsvi

Calculation of noise from railway bridges and viaducts: Experimental validation of a rapid calculation model

O.G. Bewes[a,b,*], D.J. Thompson[a], C.J.C. Jones[a], A. Wang[b]

[a]*ISVR, University of Southampton, Southampton SO17 1BJ, UK*
[b]*Pandrol Rail Fastenings Limited, 63 Station Road, Addlestone, Surrey KT15 2AR, UK*

Accepted 26 August 2005
Available online 8 February 2006

Abstract

The noise emitted by a railway bridge or viaduct under traffic can, in principle, be calculated using finite element techniques that take account of the specific geometry of the bridge, but for high frequencies, where the modal density is large, this can be very computationally intensive. This means that the benefits of performing large parametric design studies are often overshadowed by the time taken to complete them. Here, a rapid calculation model is described for the vibration power transfer from the rail into the bridge that is coupled with the SEA method for vibration power propagation and noise radiation. This relies less on the exact geometry of the bridge and more on its general characteristics. The model has recently been developed to represent the coupling between the rail and bridge at low frequencies and the mobility of the support girder at high frequencies with greater detail. It is used here to evaluate the noise and vibration of a concrete–steel composite viaduct. The predictions are then compared with real experimental noise and vibration data taken from the viaduct under traffic.

1. Introduction

The noise levels occurring when a train passes over a bridge are usually greater than those for when a train passes on normal track by up to 10 dB [1,2]. Due to the combination of road and rail traffic that exists in urban environments, many bridges can be found in heavily populated and therefore noise-sensitive areas. There is clearly a need to understand the processes behind bridge noise in order to be able to put measures in place to mitigate such noise, where appropriate.

The generation of bridge noise can be split into three steps [2]. Wheel/rail interaction causes the rail to vibrate. The vibration is then transmitted through the track fastening to the bridge structure. The energy is then transmitted throughout the various structural components of the bridge causing them to vibrate and hence radiate sound.

*Corresponding author. ISVR, University of Southampton, Southampton SO17 1BJ, UK. Fax: +44 1932 850858.
E-mail address: ob@isvr.soton.ac.uk (O.G. Bewes).

0022-460X/$ - see front matter © 2006 Elsevier Ltd. All rights reserved.
doi:10.1016/j.jsv.2005.12.016

As the fitting of rail-fastening components to an existing track form, or failure to meet noise regulations with a new track form, can be costly, it is important to be able to predict accurately the effectiveness of noise reduction techniques.

2. Approaches to the calculation of railway bridge noise

Bridge noise may be predicted using a large database of measurements from which the noise level variation with simple gross parameters can be found empirically [1]. This method is efficient computationally and suitable for some uses. However, empirically determined models do not allow design changes to be studied and it is impossible to measure novel bridge designs for which measurement data cannot be obtained. Finite element analysis is used for many aspects of bridge structure design [3]. It may be thought of as a means of providing parameters such as the point mobility required for a noise model. However, a large bridge can have many modes below even the lowest audible frequency. An approach that takes these factors into consideration is to model the bridge with an analytical track model to calculate the power input to the bridge then couple this to a simple SEA model to calculate the power distribution among the various components of the bridge. Janssens and Thompson [2] and Harrison et al. [4] both use this method to calculate the noise radiated by a number of elevated railway structures to a reasonable level of accuracy. Based on this previous work, Thompson and Jones [5] developed a model called NORBERT (Noise Of Railway Bridges and Elevated Railway structures).

The combined wheel and rail roughness is used as the input to the model. Roughness values are either used from a database or specifically measured roughness spectra can be input. Using the roughness, the vibration of the rail and wheel is calculated from the rail and wheel mobility and the speed of the rolling stock. Rail vibration is considered in the vertical direction only. The rail is modelled as a Timoshenko beam continuously supported on top of a rigid surface by a resilient layer. The force input to the bridge is assumed to be the resulting force transmitted through the resilient layer if the rail is subject to the calculated rail vibration. From this the power input to the bridge is calculated as, [2],

$$P_{\text{input}} = F^2 N \,\text{Re}\{Y_{\text{bridge}}\}, \tag{1}$$

where F^2 is the mean square force at the base of the track supports, Y_{bridge} is the point mechanical mobility of the bridge deck and N is the number of forces between the track and bridge deck.

Having calculated the total power input to the bridge structure, the distribution of power in the bridge structure is determined using a simple form of statistical energy analysis, which assumes equipartition of energy among the components of the bridge. The SEA model of the bridge structure itself is made up of only plate and beam components. Using the radiation efficiencies of each component, the total sound power radiated by the bridge is calculated. Finally, a rolling noise database is accessed that contains calculations for the rolling noise of several wheel and track combinations calculated by using the TWINS software [6,7]. The correct values are accessed and corrected for differences in the rail fastener stiffness and the rolling noise is output in terms of sound power per unit length. The sound powers radiated by the bridge, rail and wheels are then summed to give a total noise from the bridge.

A critical component for an accurate bridge noise model using the above methods is the power transfer calculation in Eq. (1) and more specifically an accurate model for the bridge mobility Y_{bridge}. In most railway bridges, box section girders or a small number of I-section beams or thick plates supports the track. In either case, an estimate of the mechanical mobility of a point on the deck of the bridge can be based upon an estimate of the average vertical mobility of an I-section beam or plate. Use is made of the result that the frequency average point mobility of a finite beam or plate can be approximated by the point mobility of an infinite beam or plate [8] and the mobility of the bridge deck is assumed to be either an infinite I-section beam or thick plate depending on the geometry, material properties and wavelengths in the bridge. Cremer and Heckl [9] present equations for the point mobility of a number of infinite structural components including an infinite Timoshenko beam and thick plate that can be used in the model. The equations in Ref. [9] give good approximations for the mobility of infinite beams assuming that no modal deformation occurs in the beam cross-section. However for beams with the typical dimensions found in bridges and viaducts, cross-sectional

deformation begins to occur at around 500 Hz [10] and a more appropriate 'high frequency' model for the beam that considers this effect is required.

Another concern with using Eq. (1) is that, at all frequencies, the force is obtained by assuming the rail is modelled as a continuously supported infinite beam on a rigid foundation with a correction for the actual discrete nature of the supports. There are three inherent problems with this assumption. Firstly, Eq. (1) assumes that the rail moves independently from the bridge at all frequencies. In reality the motion in the bridge and the rail will remain coupled up to a particular frequency known as the decoupling frequency which, for a typical bridge with very stiff rail pads, may occur above 500 Hz [11]. Therefore the assumption in Eq. (1) may be incorrect across a wide frequency band. Secondly, it has been found that assuming the motion of the rail and bridge is independent below the decoupling frequency over-estimates the power transfer into the bridge [12]. Finally, the resonance effects due to the finite length of the bridge are likely to have an important effect on the amount of power input to the bridge at low frequencies where the wavelengths in the bridge structure are long. The use of an infinite approximation for this frequency region is an over-simplification. Therefore a power transfer calculation that takes into account all these factors for frequencies below the decoupling frequency is sought.

3. An improved model for the vibrational power transfer from the rail to the bridge at low frequencies

The mean square force at the base of the track supports, used for the power input calculation in Eq. (1), is calculated assuming that the rail moves independently from the bridge at all frequencies. To improve upon this, a model of the rail and bridge as two Timoshenko beams coupled by a continuous resilient layer is considered here. The rail and bridge will act as a single composite beam up to a decoupling frequency ω_0 [11] given by,

$$\omega_0 = \sqrt{s\left(\frac{1}{\mu_s} + \frac{1}{\mu_r}\right)}, \tag{2}$$

where s is the stiffness per unit length of the track supports and μ_s and μ_r are the mass per unit length of the rail and bridge beams, respectively. It is only at frequencies higher than ω_0 that the assumption inherent in Eq. (1) is valid. Furthermore, unlike plain track, bridges are finite structures and resonance effects due to the ends of the bridge are likely to be large, particularly at low frequencies.

An improved model for the rail coupled to the bridge is described below that takes into account the coupled motion of the rail and bridge below the decoupling frequency and the resonance characteristics of the finite structure in which the track is modelled as two finite simply supported Timoshenko beams (representing the rail and bridge) continuously connected by a resilient layer (representing the track fastenings). The use of a continuous connection is justified, as the effects of the discrete supports are only significant around 1 kHz.

3.1. Equations of motion

Consider the system shown in Fig. 1 consisting of a finite Timoshenko beam of length $L = L_R + L_L$, with bending stiffness $B_s = EI_s$, representing a rail connected via an elastic layer of stiffness per unit length s to a

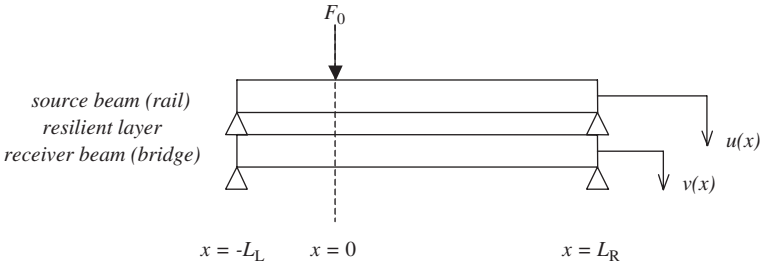

Fig. 1. Two finite Timoshenko beams connected by a continuous resilient layer used to model the rail coupled to the bridge.

second finite Timoshenko beam of equal length with bending stiffness $B_r = EI_r$, representing a bridge beam. Both beams are simply supported at $x = -L_L$ and $x = L_R$. Damping may also be included by making s, B_s and B_r complex. The system is excited at $x = 0$ by a force $F_0 e^{i\omega t}$ resulting in vertical displacement of the source and receiver beam $u(x)$ and $v(x)$, respectively. Assuming the elastic layer is soft in shear with no stiffness in the horizontal direction, only vertical motion need be considered.

Considering first a differential element of the source beam, the following set of four partial differential equations can be obtained [13]:

$$M - B_s \frac{\partial \phi}{\partial x} = 0, \tag{3}$$

$$S - \kappa_s A_s G\left(\phi - \frac{\partial u}{\partial x}\right) = 0, \tag{4}$$

$$S - \frac{\partial M}{\partial x} + \rho I_s \frac{\partial^2 \phi}{\partial t^2} = 0, \tag{5}$$

$$\frac{\partial S}{\partial x} + \mu_s \frac{\partial^2 u}{\partial t^2} + s(u - v) = 0, \tag{6}$$

where μ_s, G, A_s, ρ_s, and κ_s are the mass per unit length, shear modulus, cross-sectional area, density and shear co-efficient [14] of the beam, respectively. M is the bending moment; S the shear force acting against the shear loading and ϕ is the slope of bending in the beam. Eqs. (3) and (5) refer to the rotational motion in the element while Eqs. (4) and (6) refer to the transverse motion of the element. Eliminating S, M and ϕ, and repeating the above for the receiver beam yields the simultaneous equations of motion of the system. Assuming a solution of the form $u, v(x, t) = Ae^{\beta x} e^{i\omega t}$, the equations of motion can be written in matrix form as

$$[[A]\beta^4 + [B]\beta^2 + [C]]\begin{Bmatrix} u \\ v \end{Bmatrix} = \begin{Bmatrix} 0 \\ 0 \end{Bmatrix}, \tag{7}$$

where

$$[A] = \begin{bmatrix} B_s & 0 \\ 0 & B_r \end{bmatrix}, \tag{8}$$

$$[B] = \begin{bmatrix} \rho I_s\left(1 + \dfrac{E}{G_s\kappa_s}\right)\omega^2 - \dfrac{B_s s}{G_s A_s \kappa_s} + s & \dfrac{B_s s}{G_s A_s \kappa_s} - s \\ \dfrac{B_r s}{G_r A_r \kappa_r} - s & \rho I_r\left(1 + \dfrac{E}{G_r \kappa_r}\right)\omega^2 - \dfrac{B_r s}{G_r A_r \kappa_r} + s \end{bmatrix}, \tag{9}$$

$$[C] = \begin{bmatrix} -\mu_s\omega^2 + \dfrac{\rho^2 I_s}{G_s\kappa_s}\omega^4 + s\left(1 - \dfrac{\rho I_s \omega^2}{G_s A_s \kappa_s}\right) & -s\left(1 - \dfrac{\rho I_s \omega^2}{G_s A_s \kappa_s}\right) \\ -s\left(1 - \dfrac{\rho I_r \omega^2}{G_r A_r \kappa_r}\right) & -\mu_r\omega^2 + \dfrac{\rho^2 I_r}{G_r\kappa_r}\omega^4 + s\left(1 - \dfrac{\rho I_r \omega^2}{G_r A_r \kappa_r}\right) \end{bmatrix}. \tag{10}$$

Eq. (7) can be solved as a quadratic eigenvalue equation in β^2 to yield four eigenvalues for β^2 at each frequency. These correspond to four waves valid for $x \to \infty$ and another four $(-\beta)$ valid for $x \to -\infty$. Each has the corresponding eigenvector (u_n, v_n).

3.2. Response to a point force

The response of each beam in the system to a point force $F_0 e^{i\omega t}$ at $x = 0$ is made up of 16 wave components, as shown in Fig. 2, consisting of near-field and propagating waves travelling from the load and reflected at each end. The full solution for the displacement to the left of the forcing point (with implicit $e^{i\omega t}$ dependence)

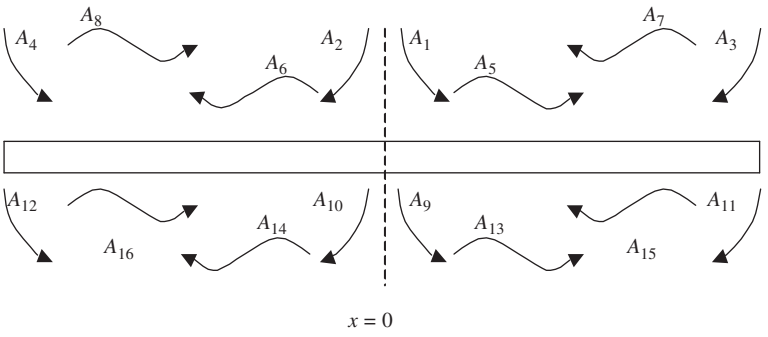

Fig. 2. The 16 wave components present in each beam.

in each beam is given by

$$u_L(x) = A_2u_1e^{\beta_1x} + A_4u_1e^{-\beta_1x} + A_6u_2e^{\beta_2x} + A_8u_2e^{-\beta_2x} + A_{10}u_3e^{\beta_3x} + A_{12}u_3e^{-\beta_3x} + A_{14}u_4e^{\beta_4x} + A_{16}u_4e^{-\beta_4x}, \tag{11}$$

$$v_L(x) = A_2v_1e^{\beta_1x} + A_4v_1e^{-\beta_1x} + A_6v_2e^{\beta_2x} + A_8v_2e^{-\beta_2x} + A_{10}v_3e^{\beta_3x} + A_{12}v_3e^{-\beta_3x} + A_{14}v_4e^{\beta_4x} + A_{16}v_4e^{-\beta_4x}. \tag{12}$$

Similarly, the displacement in each beam to the right of the forcing point is given by

$$u_R(x) = A_1u_1e^{-\beta_1x} + A_3u_1e^{\beta_1x} + A_5u_2e^{-\beta_2x} + A_7u_2e^{\beta_2x} + A_9u_3e^{-\beta_3x} + A_{11}u_3e^{\beta_3x} + A_{13}u_4e^{-\beta_4x} + A_{15}u_4e^{\beta_4x}, \tag{13}$$

$$v_R(x) = A_1v_1e^{-\beta_1x} + A_3v_1e^{\beta_1x} + A_5v_2e^{-\beta_2x} + A_7v_2e^{\beta_2x} + A_9v_3e^{-\beta_3x} + A_{11}v_3e^{\beta_3x} + A_{13}v_4e^{-\beta_4x} + A_{15}v_4e^{\beta_4x}. \tag{14}$$

Substituting Eqs. (11)–(14) in Eqs. (3)–(6) and rearranging yields the rotation angles of the rail ϕ_s and bridge ϕ_r in terms of the displacements of each wave n

$$\phi_{sn} = \frac{G_sA_s\kappa_s\beta_nu_n}{G_sA_s\kappa_s + B_s\beta_n^2 + \omega^2\rho I_s}, \qquad \phi_{rn} = \frac{G_rA_r\kappa_r\beta_nu_n}{G_rA_r\kappa_r + B_s\beta_n^2 + \omega^2\rho I_s}. \tag{15}$$

The rotation angle in each beam to the left of the forcing point is given by

$$\phi_{sL}(x) = A_2\phi_{s1}e^{\beta_1x} + A_4\phi_{s1}e^{-\beta_1x} + A_6\phi_{s2}e^{\beta_2x} + A_8\phi_{s2}e^{-\beta_2x} + A_{10}\phi_{s3}e^{\beta_3x} + A_{12}\phi_{s3}e^{-\beta_3x} + A_{14}\phi_{s4}e^{\beta_4x} + A_{16}\phi_{s4}e^{-\beta_4x}, \tag{16}$$

$$\phi_{rL}(x) = A_2\phi_{r1}e^{\beta_1x} + A_4\phi_{r1}e^{-\beta_1x} + A_6\phi_{r2}e^{\beta_2x} + A_8\phi_{r2}e^{-\beta_2x} + A_{10}\phi_{r3}e^{\beta_3x} + A_{12}\phi_{r3}e^{-\beta_3x} + A_{14}\phi_{r4}e^{\beta_4x} + A_{16}\phi_{r4}e^{-\beta_4x}. \tag{17}$$

The rotation angle in each beam to the right of the forcing point is given by

$$\phi_{sR}(x) = A_1\phi_{s1}e^{-\beta_1x} + A_3\phi_{s1}e^{\beta_1x} + A_5\phi_{s2}e^{-\beta_2x} + A_7\phi_{s2}e^{\beta_2x} + A_9\phi_{s3}e^{-\beta_3x} + A_{11}\phi_{s3}e^{\beta_3x} + A_{13}\phi_{s4}e^{-\beta_4x} + A_{15}\phi_{s4}e^{\beta_4x}, \tag{18}$$

$$\phi_{rR}(x) = A_1\phi_{r1}e^{-\beta_1x} + A_3\phi_{r1}e^{\beta_1x} + A_5\phi_{r2}e^{-\beta_2x} + A_7\phi_{r2}e^{\beta_2x} + A_9\phi_{r3}e^{-\beta_3x} + A_{11}\phi_{r3}e^{\beta_3x} + A_{13}\phi_{r4}e^{-\beta_4x} + A_{15}\phi_{r4}e^{\beta_4x}. \tag{19}$$

The unknown wave amplitudes A_n can be found by applying the following boundary conditions:

(a) Continuity of displacement at $x = 0$.

$$u_L(0) = u_R(0), \quad v_L(0) = v_R(0). \tag{20}$$

(b) Continuity of rotation at $x = 0$.

$$\phi_{sL}(0) = \phi_{sR}(0), \quad \phi_{rL}(0) = \phi_{rR}(0). \tag{21}$$

(c) Continuity of bending moment at $x = 0$.

$$\beta_n\phi_{sL}(0) = \beta_n\phi_{sR}(0), \quad \beta_n\phi_{rL}(0) = \beta_n\phi_{rR}(0). \tag{22}$$

(d) Displacement at the beam ends.

$$u_L(-L_L) = u_R(L_R) = v_L(-L_L) = v_R(L_R) = 0. \tag{23}$$

(e) Bending moment at the beam ends.

$$\beta_n\phi_{sL}(-L_L) = \beta_n\phi_{sR}(L_R) = \beta_n\phi_{rL}(-L_L) = \beta_n\phi_{rR}(L_R) = 0. \tag{24}$$

(f) Equating shear forces at $x = 0$.

$$\frac{S_s(0)}{G_sA_s\kappa_s} = (\phi_{sn} + \beta_n u_n) = \frac{F}{2G_sA_s\kappa_s}, \quad \frac{S_r(0)}{G_rA_r\kappa_r} = (\phi_{rn} + \beta_n v_n) = 0. \tag{25}$$

Substitution of Eqs. (11)–(19) into Eqs. (20)–(25) yields 16 simultaneous equations that can be solved using the matrix method to find the unknown wave amplitudes. Hence the full solutions for the displacement in each beam can be found.

3.3. Calculation of the power input to the bridge

The power input to a structure due to the action of a point force is given by the real part of the mobility of the structure multiplied by the mean square force amplitude

$$P_{\text{in}} = \tfrac{1}{2}|F|^2\,\text{Re}\{Y\}, \tag{26}$$

where Y is the mobility of the structure.

The theory in Sections 3.1–3.2 gives a method for calculating the response of the track mounted to a bridge to a point force at the track. The mobility for each system can readily be calculated and the force is evaluated from the wheel/rail interaction. Hence the total power input to the lower beam can be found as

$$P_{\text{in}} = \frac{1}{2}\,\text{Re}\int_{-L_L}^{L_R} F^*(x)\dot{v}(x)\,\mathrm{d}x = \frac{1}{2}\,\text{Re}\int_{-L_L}^{L_R} (s(u(x) - v(x)))^*\dot{v}(x)\,\mathrm{d}x, \tag{27}$$

where F^* is complex conjugate of the force applied to the bridge beam through the stiffness s of the resilient layer and $\dot{v}$ is the velocity of the bridge beam.

3.4. Results

The model described above was used to obtain values for the real part of the driving point mobility at the rail head and the power input to the bridge at discrete frequencies in the range 1 Hz–5 kHz. The technical data for the beams used in the model are shown in Table 1. The rail pad stiffness per unit length, s, was $2 \times 10^8\,\text{N/m}^2$ with a loss factor 0.25. This is typical of fastener systems used on a bridge [15].

Frequency response functions are plotted in Fig. 3 along with results for infinite beams. Considering first the driving point mobility (Fig. 3(a)) for the infinitely long model, at low frequencies the vibration in the rail and bridge beams is coupled and the mobility tends to that of the combined rail and bridge beams. The mobility begins to rise at approximately 20 Hz as the motion in the beams starts to become uncoupled. There is a peak in the mobility at approximately 300 Hz. This corresponds to the decoupling frequency as given in Eq. (2). At frequencies above the decoupling frequency, the motion in the two beams is weakly coupled. As frequency

Table 1
Properties of beams used in the models

	Rail beam	Bridge beam
μ (kg/m)	54	499
L (m)	16	16
I (m^4)	2.4×10^{-5}	9.33×10^{-3}
E (N/m^2)	2.07×10^{11}	2.07×10^{11}
κ	0.4	0.6

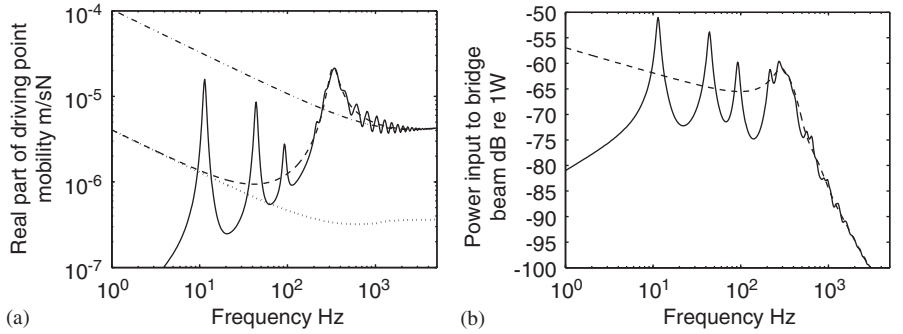

Fig. 3. Real part of the driving point mobility against frequency at the rail head (a) and power input to the bridge beam for a 1 N input force on the rail (b). —, two finite Timoshenko beams joined by a resilient layer; — —, two infinite Timoshenko beams joined by a resilient layer; • • •, combined rail and bridge beams modelled as Timoshenko beams; — • —, rail modelled as a Timoshenko beam.

increases further, the mobility tends to that of the rail. Now consider the point mobility of the finite case (solid line), taken at 4 m along the span of length 16 m. It can be seen that the overall trends of the mobility are as for the infinite beams. However, the fundamental bending mode and higher order modes of the bridge beam can be seen in the response below the decoupling frequency. The modal density above the decoupling frequency is too high to identify the individual modes due to the short wavelengths in the rail.

Looking now at the power input to the bridge (Fig. 3(b)), for the infinite beam the power input to the bridge decreases slowly with increasing frequency from 1 to 100 Hz. There is a peak at the decoupling frequency, above which the power input to the bridge decreases rapidly with increasing frequency, as the bridge is isolated from the rail. The resonances of the bridge treated as a finite structure again follow the same trend, but it will be noted that below the decoupling frequency, individual resonances cause up to 10 dB departure from the infinite beam behaviour.

4. An improved model for the mobility of a bridge at high frequencies

For the power input calculation in Eq. (1) the point mobility of the bridge can be represented as either an infinite I-section beam or infinite thick plate. The thick plate model is only used if the lateral distance of the input force from the web of any support girder is greater than one-quarter of a bending wavelength in the deck. In many cases this means that the I-section beam mobility model is used up to very high frequencies. As discussed above, the infinite beam equations given in Ref. [9] do not give accurate results at such high frequencies due to the local deformation that occurs within the cross-section of the beam. Ref. [10] shows a method devised to model accurately the mobility of an infinite I-section beam in three frequency ranges. In a similar way to Ref. [2], at low frequencies the I-section beam is modelled as an infinite or finite Timoshenko beam as in Ref. [9]. A detailed finite element study of various finite I-section beams identified a mode that occurs in I-section beams at high frequencies that is independent of the length of the beam and corresponds to the first occurrence of longitudinal waves within the depth of the beam. The mode, labelled the ‘transitional’ mode marks a distinct change in the behaviour of the beam where the mobility begins to behave as the

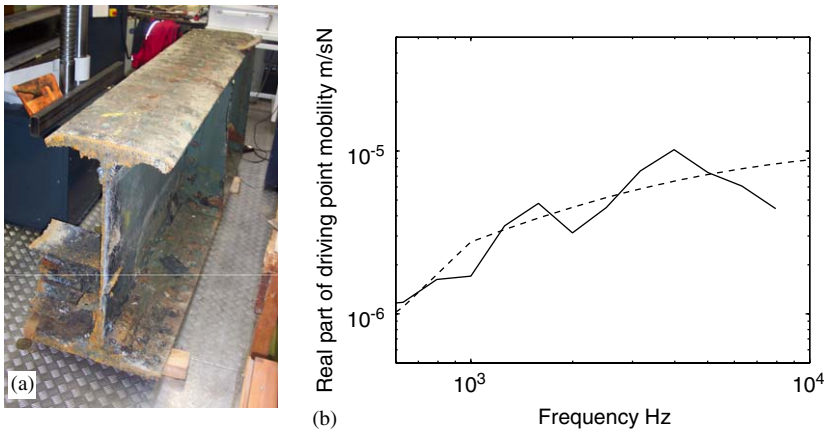

Fig. 4. A 3 m length of a wrought iron I-section beam removed from a BR bridge (a). The real part of the driving point mobility of a 3×1 m I-section beam with a 45 cm flange (b): —, measured; — —, predicted.

mobility of an edge-excited flat plate. An in-depth study of the behaviour of the beam at frequencies above the transitional mode using a combination of finite element, boundary element and dynamic stiffness methods led to the derivation of a high frequency infinite beam mobility given by [10]

$$Y_{\text{bridge}} \approx \left[\frac{1}{(\omega/4)((1-\nu^2)/Eh_w) + (1/\rho c_R^2 h_w)} + 8\sqrt{\frac{I_f E \rho h_f}{1-\nu^2}} \right]^{-1}, \tag{28}$$

where E, ρ and ν are the Young's modulus, density and Poisson's ratio of the beam, c_R is the Rayleigh wave speed in the beam, h_w and h_f are the thickness of the beam web and flange and $I_f = h_f^3/12$ is the second moment per unit width of area of the flange. The first term in Eq. (28) is the mobility of an edge-excited flat plate as derived by Pinnington [16], modified to take better account of the edge of the plate. The second term of Eq. (28) is the mobility of the flange modelled as a normally excited infinite flat plate as in Ref. [9].

At mid-frequencies, the mobility of the I-section beam was seen to behave neither like a beam nor an edge-excited flat plate. In this 'transitional' region, the mobility is seen to increase with the square of frequency up to the transitional mode value [10]. This simple approach was found to describe the mobility in this range well for a large number of test cases.

Mobility measurements have been performed on a short section of an I-section beam removed from an old wrought iron railway bridge typical of many across the UK, Fig. 4. The beam is approximately 3 m long and 1 m deep with a 0.4 m wide flange. The thickness of the flange and web, respectively, are approximately 0.04 and 0.03 m. The point mobility was measured at a number of points above the web along the length of the beam. The point mobility was then averaged over all the positions. The average real part of the driving point mobility is plotted from 600 to 8000 Hz in Fig. 4 together with the prediction of the model from [10]. In the prediction, Eq. (28) applies above 1 kHz and the 'transitional' region is below this frequency. The measured results fluctuate around the predicted mobility due to flange resonances, but the mean mobility is well predicted. Results are not shown at lower frequencies due to the influence of the short length of the beam.

5. Testing of the improved model using noise and vibration measurements from a steel–concrete composite viaduct under traffic

This section is concerned with the validation of the bridge noise model described in Section 2 after modification to include the improvements described. Validation was performed using noise and vibration data taken from an existing viaduct under traffic together with mobility measurements at the rail head.

5.1. Test site and method

A diagram of the cross-section is shown in Fig. 5. It consists of an 8m wide concrete deck of thickness 0.4 m supported by two steel I-section beams of 1 m depth with a 0.4 m wide flange. The thickness of the webs and flanges are 0.03 and 0.02 m, respectively. The viaduct supports two straight sections of track directly fastened at 0.6 m intervals to the concrete deck via resilient rail pads with a stiffness of between 1×10^8 and 2×10^8 N/m. The viaduct also has a 1 m high noise barrier running parallel to one of the tracks. The traffic at the test site consisted wholly of light rail traffic with an average speed of 52 km/h, each train being 56 m long and made up of four cars.

Firstly, a series of mobility measurements were performed on the bridge in order to determine the driving point mobility at the rail head for comparison with the finite Timoshenko beam model described in Section 3 and to determine the stiffness and damping properties of the viaduct. The mobility was measured at points directly above the track fasteners and at mid-span between two fasteners and an average was taken.

Vibration measurements under traffic were made at two positions along the span of the viaduct (centre-span and quarter-span). The accelerometer positions at each point on the span are shown in Fig. 5(a). Rail vibration was measured at each rail foot on one track (1. and 2. in Fig. 5). Deck vibration was measured at the track-centre (4. in Fig. 5) and at a position near the outer edge of the viaduct (3. in Fig. 5). Noise recordings were also made at a position 5 m directly beneath the viaduct. Recordings were made digitally using a laptop PC running at a sampling frequency of 12 kHz during the passing of 48 trains.

5.2. Results and model validation

5.2.1. Mobility

A problem when predicting the noise and vibration from existing bridges and viaducts is that many of the parameters needed are not known, such as the stiffness of the track supports and damping in the various components. In the case of the test viaduct, only the dimensions and materials properties are known. With the use of a track model, such as the one described in Section 3, curve fitting can be used to extract important parameters for use in noise and vibration predictions of the viaduct.

Fig. 5(b) shows a plot of the magnitude of the driving point mobility at the rail head against frequency measured close to the centre of the viaduct. Results are presented within the frequency range 80–800 Hz. Signal-to-noise problems prevented measurement of the mobility outside of this frequency range. However the range is adequate in order to extract the required parameters for input to the model. The peak at approximately 310 Hz corresponds to the decoupling frequency as described in Eq. (2). Also plotted in Fig. 5(b) is the spatially averaged magnitude of the driving point mobility predicted using the model described

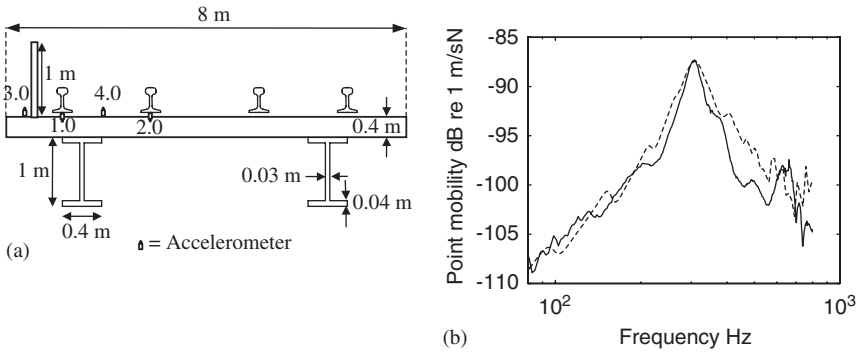

Fig. 5. A diagram of the viaduct cross-section and vibration measurement positions (a). The magnitude of the driving point mobility measured at the rail head (b). —, measured; — —, predicted.

in Section 3. The material and geometrical properties of the bridge are known and s is calculated by fitting the predicted mobility curve to the measured results. This gives a value of 8.4×10^7 N/m.

Considering again the measured mobility, from 80 Hz to the decoupling frequency the mobility resembles the region where the rail and bridge motion are becoming uncoupled (Fig. 5(a)). In this region no prominent bending modes in the bridge are seen, suggesting high damping in the bridge. For higher frequencies the measured mobility resembles the region where the mobility tends towards that of the rail alone. Although no individual modes can be seen, the peaks and troughs in the mobility suggest that the finite length of the bridge affects the mobility even at high frequencies.

5.2.2. Noise and vibration

The spatially averaged vibration velocity on the deck has been calculated by averaging the measured vibration at each measurement position for all 48 trains. The results are plotted in one-third octave bands together with the range of results seen in the tests in Fig. 6(a). Using the improved model of Sections 3 and 4, the predictions of the spatially averaged deck vibration are obtained and also plotted in Fig. 6(a). The input parameters for the model were the known geometrical and material properties for the bridge, typical light rail parameters for the rolling stock and, as no wheel or rail roughness measurements were taken in this test, an average UK rail/wheel roughness has been used as excitation input [17].

It can be seen in Fig. 6(a) that the model predicts the deck vibration well between 50 Hz and 1 kHz with errors of no more than 4 dB at discrete frequency bands. For frequencies less than 50 Hz the model under-predicts the average deck vibration. This is likely to be due to the use of an assumed wheel/rail roughness as well as limitations of the SEA model at low frequencies. For frequencies higher than 1 kHz the predicted deck vibration diverges from the measured results. It is possible that this is again due to the assumed roughness spectra. Furthermore, due to the high dynamic range of the measured vibration and high level of isolation at high frequencies the measured results are expected to be less reliable.

The average sound pressure level measured underneath the viaduct for the 48 trains is plotted in Fig. 6(b) together with the range of levels seen in the tests. The sound power predictions for the viaduct have been converted to a total sound pressure spectrum by considering viaduct as line source [18]. The results are also plotted in Fig. 6(b). It can be seen that the errors in the noise predictions are larger than for the deck vibration predictions at some discrete frequency bands. However, the predictions are within the 4 dB levels measured in the test at most frequencies up to approximately 600 Hz. Again, errors in this frequency range are expected to be due to an assumed roughness spectrum used as the input excitation. Above 600 Hz the noise level predicted using the model rolls off sharply while the measured spectrum rolls off less sharply. The spatially averaged deck vibration predictions shown in Fig. 6(a) diverge from measurements at approximately 1 kHz. Therefore under-prediction of the noise radiated by the bridge at high frequencies is expected. Furthermore, the prediction shown in Fig. 6(b) is for the noise radiated by the bridge structure alone and takes no account of other sources such as the rolling noise. It is likely that the measured spectrum contains a contribution from the rolling noise at high frequencies.

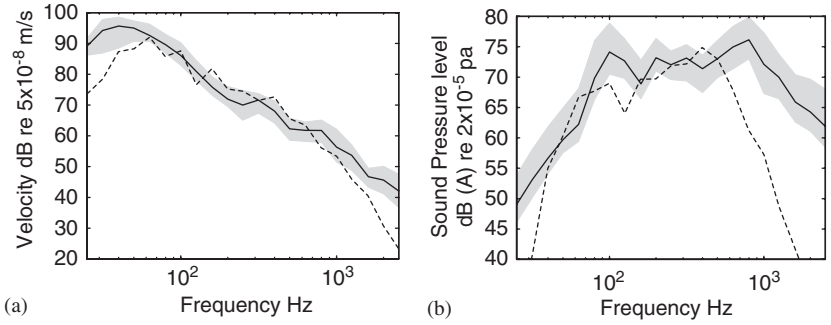

Fig. 6. The spatially averaged vibration on the bridge deck (a) and the sound pressure level (b) measured 5 m below the viaduct. —, measured average; — —, predicted.

6. Conclusions and further work

A bridge noise calculation model has been presented that, with modification to the track model at low frequencies and the model for the mobility of the bridge at high frequencies, rapidly predicts average deck vibration and sound pressure level radiated by the bridge with a reasonable level of accuracy between 40 Hz and 1 kHz. It is thought that an improved level of accuracy could be achieved if a measured wheel/rail roughness spectrum could be used. The model has no requirement of detailed finite element calculations and takes less than 1 min to run in this case.

The test case described consisted of a very simply constructed viaduct and the track was directly fastened to the viaduct. The track model described in Section 3 has the capability for modelling track configurations with more than one layer of fastening stiffness, such as resilient baseplates or ballasted track. Therefore it is desirable to perform further validation of the models on more complex viaducts with different track configurations.

References

[1] L.G. Kurzweil, Prediction and control of noise from railway bridges and tracked transit elevated structures, *Journal of Sound and Vibration* 51 (1977) 419–439.
[2] M.H.A. Janssens, D.J. Thompson, A calculation model for noise from steel railway bridges, *Journal of Sound and Vibration* 193 (1996) 295–305.
[3] A.R. Crockett, J. Pyke, Viaduct design for minimisation of direct and structure-radiated train noise, *Journal of Sound and Vibration* 231 (2000) 883–897.
[4] M.F. Harrison, D.J. Thompson, C.J.C. Jones, The calculation of noise from railway viaducts and bridges, *Proceedings of the IMechE* 214 (Part F) (2000) 125–134.
[5] D.J. Thompson, C.J.C. Jones, NORBERT—software for predicting the noise of railway bridges and elevated structures, ISVR Contract Report, No. 02/24, November 2002.
[6] D.J. Thompson, B. Hemsworth, N. Vincent, Experimental validation of the TWINS prediction program for rolling noise, Part 1: description of the model and method, *Journal of Sound and Vibration* 193 (1996) 123–136.
[7] D.J. Thompson, P. Fodiman, H. Mahé, Experimental validation of the TWINS prediction program for rolling noise, Part 2: results, *Journal of Sound and Vibration* 193 (1996) 137–148.
[8] E. Skurdrzyk, The mean-value method of predicting the dynamic response of complex vibrators, *Journal of Acoustic Society of America* 67 (1980) 1105–1135.
[9] L. Cremer, M. Heckl, E.E. Unger, *Structure-Borne Sound*, second ed., Springer, Berlin, 1988.
[10] O. Bewes, D.J. Thompson, C.J.C. Jones, Calculation of noise from railway bridges: the mobility of beams at high frequencies, *Proceedings of the Eighth International Conference on Recent Advances in Structural Dynamics*, Southampton, England, 2003.
[11] D.J. Thompson, An analytical model for the vibration isolation for a rail mounted on a bridge, TNO Report, TPD-HAG-RPT-92-0069, May 1992.
[12] O. Bewes. The Calculation of Noise from Railway Bridges and Viaducts, Engineering Doctorate Mini-Thesis, University of Southampton, 2003.
[13] J.F. Doyle, *Wave Propagation in Structures*, second ed., Springer, Berlin, 1997.
[14] G.R. Cowper, The shear coefficient in Timoshenko's beam theory, *Journal of Applied Mechanics* June (1966) 335–340.
[15] D.J. Thompson, J.W. Verheij, The dynamic behaviour of rail fasteners at high frequencies, *Applied Acoustics* 52 (1997) 1–15.
[16] R.J. Pinnington, Approximate mobilities of built up structures, ISVR Technical Report No. 162, 1988.
[17] A.E.J. Hardy, Draft proposal for noise measurement standard for ERRI committee C163, Report RR-SPS-97-012 of AEAT Rail Ltd., European Rail Research Institute, 1997.
[18] D.A. Bies, C.H. Hansen, *Engineering Noise Control: Theory and Practice*, third ed., Spon Press, London, 2003.